J. Fluid Mech. (2025), *vol.* 1019, A5, doi:10.1017/jfm.2025.10571

Transient growth in streaky unbounded shear flow: a symbiosis of Orr and push-over mechanisms

William Oxley[1] **and Rich R. Kerswell**[1]

[1]DAMTP, Centre for Mathematical Sciences, Wilberforce Road, Cambridge CB3 0WA, UK

Corresponding author: William Oxley, woo21@cam.ac.uk

(Received 7 March 2025; revised 27 June 2025; accepted 4 August 2025)

Transient growth mechanisms operating on streaky shear flows are believed important for sustaining near-wall turbulence. Of the three individual mechanisms present – Orr, lift-up and 'push over' – Lozano-Duran *et al.* 2021 (*J. Fluid Mech.* **914**, A8) have recently observed that both Orr and push over need to be present to sustain turbulent fluctuations given streaky (streamwise-independent) base fields whereas lift-up does not. We show here, using Kelvin's model of unbounded constant shear augmented by spanwise-periodic streaks, that this is because the push-over mechanism can act in concert with a Orr mechanism based upon the streaks to produce much-enhanced transient growth. The model clarifies the transient growth mechanism originally found by Schoppa & Hussain (2002 *J. Fluid Mech.* **453**, 57–108) and finds that this is one half of a linear instability mechanism centred at the spanwise inflexion points observed originally by Swearingen & Blackwelder (1987 *J. Fluid Mech.* **182**, 255–290). The instability and even transient growth acting on its own are found to have the correct nonlinear feedback to generate streamwise rolls which can then re-energise the assumed streaks through lift-up indicating a sustaining cycle. Our results therefore support the view that, while lift-up is believed central for the roll-to-streak regenerative process, it is Orr and push-over mechanisms that are both key for the streak-to-roll regenerative process in near-wall turbulence.

Key words: turbulent boundary layers, shear-flow instability

1. Introduction

Efforts to understand wall-bounded turbulence have naturally focussed on the wall and the (coherent) structures which form there (Richardson 1922). The consensus is that there is (at least) a near-wall sustaining cycle (Hamilton, Kim & Waleffe 1995; Waleffe 1997;

© The Author(s), 2025. Published by Cambridge University Press. This is an Open Access article, distributed under the terms of the Creative Commons Attribution licence (https://creativecommons.org/licenses/by/4.0/), which permits unrestricted re-use, distribution and reproduction, provided the original article is properly cited.

https://doi.org/10.1017/jfm.2025.10571 Published online by Cambridge University Press

Jimenez & Pinelli 1999; Farrell & Ioannou 2012) involving predominantly streaks and streamwise rolls (or vortices) which helps maintain the turbulence (e.g. see the reviews Robinson 1991; Panton 2001; Smits, McKeon & Marusic 2011; Jimenez 2012, 2018). The generation of these streaks from the rolls is commonly explained by the (linear) transient growth 'lift-up' mechanism (Ellingsen & Palm 1975; Landahl 1980), but how rolls are regenerated from the streaks has proven a little less clear due to the need to invoke nonlinearity at some point.

Just focusing on the initial linear part, Schoppa & Hussain (2002) suggested that transient growth mechanisms on the streaks were actually more important than (linear) streak instabilities, and that it was these transiently growing perturbations which fed back to create streaks through their nonlinear interaction. While this view has been contested (e.g. Hoepffner, Brandt & Henningson 2005; Cassinelli, De Giovanetti & Hwang 2017; Jimenez 2018), it is supported by recent cause-and-effect numerical experiments by Lozano-Durán *et al.* (2021), who looked more closely at all the linear processes present. In particular, Lozano-Durán *et al.* (2021) isolated the influence of the three different transient growth mechanisms: the familiar Orr (Orr 1907) and lift-up (Ellingsen & Palm 1975) mechanisms present for a one-dimensional flow profile $U(y)$ and a far less-studied 'push-over' mechanism which can only operate when the base profile has spanwise shear i.e. $U(y, z)$. They found, somewhat unexpectedly, that the Orr and push-over mechanisms are both essential to maintain near-wall turbulence when streaky base flows were prescribed but lift-up is not: see their § 6.4 and figure 24(*a*).

Markeviciute & Kerswell (2024) investigated this further by looking at the transient growth possible on a wall-normal shear plus monochromatic streak field consistent with the buffer region at the wall. Over appropriately short times (e.g. one eddy turnover time, as proposed by Butler & Farrell (1993)), they found a similarly clear signal that lift-up is unimportant whereas the removal of push over dramatically reduced the growth: see their figure 7. The necessity to have push over operating with the Orr mechanism indicates they are working symbiotically. How this happens, however, is puzzling from the time scale perspective as Orr is considered a 'fast' mechanism which operates over inertial time scales whereas push over looks a 'slow' mechanism operating over viscous time scales. This latter characterisation comes from an analogy with lift-up in which viscously decaying wall-normal velocities (as present in streamwise rolls) advect the base shear to produce streaks. Push over (a term coined by Lozano-Durán *et al.* (2021)) similarly involves viscously decaying spanwise velocities advecting the spanwise streak shear. Understanding exactly how these two mechanisms constructively interact is therefore an interesting issue.

The purpose of this paper is to lay bare this interaction by exploring it in an augmented version of Kelvin's famous constant-shear model (Kelvin 1887). This simple model – an unbounded shear $\boldsymbol{U} = y\hat{\boldsymbol{x}}$ (just the red flow in figure 1) – was used by Orr (1907) for his seminal work and has been important in clarifying the characteristics of both Orr and lift-up mechanisms subsequently (e.g. Farrell & Ioannou 1993; Jimenez 2013; Jiao *et al.* 2021) and as a shear-flow testbed otherwise (e.g. Moffatt 1967; Marcus & Press 1977). The key features of the model are that the base flow is: (i) unbounded and so not restricted by any boundary conditions; and (ii) a linear function of space. These together permit plane wave solutions to the perturbation evolution equations where the spatially varying base advection can be accounted for by time-dependent wavenumbers. This leaves just 2 ordinary differential equations (ODEs) for the cross-shear velocity and cross-shear vorticity to be integrated forward in time. These 'Kelvin' modes form a complete set but, unusually, are not individually separable in space and time and so the representation differs from the usual plane wave approach with constant wavenumbers. Kelvin and Orr used

https://doi.org/10.1017/jfm.2025.10571 Published online by Cambridge University Press

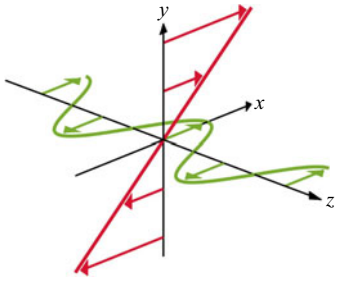

Figure 1. The streaky unbounded shear flow studied here: see (2.1). The (green) spanwise streaks extend Kelvin's (red) popular constant-shear model.

these modes to study unidirectional shear but they can also be used more generally to study the stability of time-dependent spatially linear flows (Craik & Criminale 1986; Craik 1989), flows with closed streamlines such as elliptical (Bayly 1986; Landman & Saffman 1987; Waleffe 1990) and precessing flows (Kerswell 1993), or flows with more physics included such as stratification (Hartman 1975; Miyazaki & Fukumoto 1992), rotation (Tung 1983; Leblanc & Cambon 1997; Salhi & Cambon 2010), magnetic fields (Craik 1988) or elasticity (Lagnado, Phan-Thien & Leal 1985).

The augmented base flow considered here – shown in figure 1 and (2.1) – builds in a streak field which introduces spatially periodic spanwise shear. This is now not purely linear in space and so a Kelvin mode is no longer a solution of the linearised perturbation equations. Instead, a single sum of Kelvin modes over spanwise wavenumbers is needed, but, importantly, the wall-normal shear can be handled as usual, removing the unbounded advective term from the system. This means the model system is still a very accessible 'sandbox' in which to study the transient growth mechanisms of Orr, lift-up and now, crucially, also 'push over'. The price to be paid for introducing the streak field is an order of magnitude increase in the number of ODEs to be solved, but, since this is increased from 2 to $O(20)$, it is trivial by today's standards.

The plan of the paper is as follows. Section 2 introduces the model, the evolution equations and discusses appropriate parameter values. Section 3 revisits Kelvin's unbounded constant-shear model, presenting some new large-Re asymptotic scaling laws (where Re is the Reynolds number) and discussing the timescales for Orr and lift-up growth mechanisms. The presence of streaks is introduced in § 4, with the two-dimensional (2-D) limit of no streamwise variation used in § 4.1 to illustrate how the push-over mechanism behaves when it acts alone. This is followed by a general analysis of the transient growth possible for the full 3-D system in § 4.2 which is found to clearly capture the symbiotic relationship between Orr and push over. Section 4.3 then describes a severely truncated two-variable system which contains the essence of how Orr and push over help each other to generate enhanced growth. Sections 4.4 and 4.5 discuss the energy growth possible in this system which is centred on a linear instability mechanism. Section 4.6 discusses how this linear instability becomes only transient when diffusion is reinstated and derives some simple estimates for the transient energy growth possible which match well with what is found in the full 3-D system. Section 4.7 shows that the two-variable system does not nonlinearly drive any streamwise rolls and so motivates examination of a more realistic three-variable system in § 4.8 which does. Section 4.9 explains why lift up hampers the enhanced growth produced by push over and Orr working together and § 4.10 relates the results to previous work considering the full Navier–Stokes equations in a realistic geometry. A final discussion follows in § 5.

https://doi.org/10.1017/jfm.2025.10571 Published online by Cambridge University Press

2. Formulation

2.1. *Governing equations*

We consider a unidirectional base flow velocity in the x-direction which has a constant shear in y and a spatially periodic 'streak' shear varying in the spanwise z-direction

$$\boldsymbol{U}_B = U_B(y, z)\boldsymbol{e}_x = [y + \beta \cos(k_z z)]\boldsymbol{e}_x, \tag{2.1}$$

where β is the dimensionless streak strength: see figure 1. The system has been non-dimensionalised by the y-shear rate, S, and the initial k_y wavenumber (i.e. by a length scale $L := L_y/2\pi$ where L_y is the initial perturbation wavelength in y), so that the streak wavenumber k_z is a parameter of the problem. This allows straightforward access to the well-studied Kelvin problem of $\beta \to 0$ while using the spanwise wavenumber as an inverse length scale does not.

The Navier–Stokes equations linearised around $\boldsymbol{U}_B$ for a perturbation $\boldsymbol{u} := (u, v, w)$ and associated pressure perturbation p are then

$$\frac{\partial \boldsymbol{u}}{\partial t} + [y + \beta \cos(k_z z)]\frac{\partial \boldsymbol{u}}{\partial x} + [v - \beta w k_z \sin(k_z z)]\boldsymbol{e}_x + \nabla p = \frac{1}{Re}\Delta \boldsymbol{u}, \tag{2.2}$$

$$\nabla \cdot \boldsymbol{u} = 0. \tag{2.3}$$

Here, the Reynolds number is $Re := L^2 S/\nu$, where ν is the kinematic viscosity. Taking $\boldsymbol{e}_y \cdot \nabla \times \nabla \times$ and $\boldsymbol{e}_y \cdot \nabla \times$ of (2.2) leads to a pair of equations for v and the y-shearwise vorticity $\eta := \partial u/\partial z - \partial w/\partial x$, respectively,

$$\left[\frac{\partial}{\partial t} + [y + \beta \cos(k_z z)]\frac{\partial}{\partial x} - \frac{1}{Re}\Delta\right]\Delta v + 2\beta k_z \sin(k_z z)\left[\frac{\partial^2 w}{\partial x \partial y} - \frac{\partial^2 v}{\partial x \partial z}\right] - \beta k_z^2 \cos(k_z z)\frac{\partial v}{\partial x} = 0, \tag{2.4}$$

$$\left[\frac{\partial}{\partial t} + [y + \beta \cos(k_z z)]\frac{\partial}{\partial x} - \frac{1}{Re}\Delta\right]\eta + \frac{\partial v}{\partial z} + \beta k_z \sin(k_z z)\frac{\partial v}{\partial y} - \beta w k_z^2 \cos(k_z z) = 0. \tag{2.5}$$

2.2. *Kelvin modes*

The well-known trick to handle the y-dependent advection term is to allow the wavenumbers of the perturbation to be time-dependent (Kelvin 1887) giving a 'Kelvin' mode

$$[u, v, w, p, \eta](x, y, z, t) = [\hat{u}, \hat{v}, \hat{w}, \hat{p}, \hat{\eta}](t)\mathrm{e}^{\mathrm{i}[k_x x + (1 - k_x t)y + k_z z]}, \tag{2.6}$$

which is actually a full solution to the unlinearised perturbation equations since $\boldsymbol{k} \cdot \boldsymbol{u} = 0$ by incompressibility (e.g. Craik & Criminale 1986). For $\beta \neq 0$, the extra streak shear unavoidably couples different spanwise wavenumbers and the perturbation ansatz has to be extended to

$$[u, v, w, p, \eta](x, y, z, t) = \sum_{m=-M}^{M} [\hat{u}_m, \hat{v}_m, \hat{w}_m, \hat{p}_m, \hat{\eta}_m](t)\mathrm{e}^{\mathrm{i}[k_x x + (1 - k_x t)y + m k_z z]}, \tag{2.7}$$

where, formally, M should be infinite but, practically, is chosen large enough so as not to influence the results. This ansatz could be extended further by shifting the spanwise wavenumbers by a fraction of the base wavenumber – so $mk_z \to mk_z + \mu$

https://doi.org/10.1017/jfm.2025.10571 Published online by Cambridge University Press

where $-(1/2)k_z \leqslant \mu < (1/2)k_z$ is the modulation parameter in Floquet theory – but only $\mu = 0$ is treated here so the perturbation has the same wavelength as the base field (i.e. there is no modulation) consistent with numerical observations e.g. Schoppa & Hussain (2002). Also, since $\boldsymbol{U}_B$ is symmetric about $z = 0$, perturbations which are either symmetric ('varicose') or antisymmetric ('sinuous') in u about $z = 0$ can be pursued separately. However, the computations are sufficiently low-cost that it was easier to just consider both cases together.

The continuity equation and definition of η make it possible to express $\hat{u}_m$ and $\hat{w}_m$ in terms of $\hat{v}_m$ and $\hat{\eta}_m$ as follows:

$$\hat{u}_m = \frac{-k_x(1-k_x t)\hat{v}_m - \mathrm{i}mk_z\hat{\eta}_m}{k_x^2 + m^2k_z^2} \quad \text{and} \quad \hat{w}_m = \frac{-mk_z(1-k_x t)\hat{v}_m + \mathrm{i}k_x\hat{\eta}_m}{k_x^2 + m^2k_z^2}, \tag{2.8}$$

and then (2.4) and (2.5) require for each integer m

$$\begin{aligned}\dot{\hat{v}}_m + \left[-\frac{2k_x(1-k_x t)}{k_m^2} + \frac{k_m^2}{Re}\right]\hat{v}_m = {} & \frac{\mathrm{i}\beta k_x}{2k_m^2}\left[2(m+1)\frac{k_z^2k_{m+1}^2}{h_{m+1}^2} - k_z^2 - k_{m+1}^2\right]\hat{v}_{m+1} \\ & - \frac{\mathrm{i}\beta k_x}{2k_m^2}\left[2(m-1)\frac{k_z^2k_{m-1}^2}{h_{m-1}^2} + k_z^2 + k_{m-1}^2\right]\hat{v}_{m-1} \\ & + \frac{\beta k_x^2k_z(1-k_x t)}{k_m^2h_{m+1}^2}\hat{\eta}_{m+1} - \frac{\beta k_x^2k_z(1-k_x t)}{k_m^2h_{m-1}^2}\hat{\eta}_{m-1},\end{aligned} \tag{2.9}$$

and

$$\begin{aligned}\dot{\hat{\eta}}_m + \frac{k_m^2}{Re}\hat{\eta}_m = {} & -\frac{\mathrm{i}k_x\beta}{2}\left(1 - \frac{k_z^2}{h_{m+1}^2}\right)\hat{\eta}_{m+1} - \frac{\mathrm{i}k_x\beta}{2}\left(1 - \frac{k_z^2}{h_{m-1}^2}\right)\hat{\eta}_{m-1} \\ & - \mathrm{i}mk_z\hat{v}_m - \frac{\beta k_z(1-k_x t)}{2}\left(\frac{(m+1)k_z^2}{h_{m+1}^2} - 1\right)\hat{v}_{m+1} \\ & - \frac{\beta k_z(1-k_x t)}{2}\left(\frac{(m-1)k_z^2}{h_{m-1}^2} + 1\right)\hat{v}_{m-1},\end{aligned} \tag{2.10}$$

where $h_m^2 := k_x^2 + m^2k_z^2$ and $k_m^2 := k_x^2 + (1-k_x t)^2 + m^2k_z^2$. These $2(2M+1)$ coupled complex ODEs are readily integrated forward in time from given initial conditions using MATLAB's ode45.

2.3. *Kinetic energy and optimal gain*

The volume-averaged kinetic energy is defined as

$$E(t) := \frac{1}{V_\Omega}\int_\Omega \frac{1}{2}|\boldsymbol{u}(\mathbf{x}, t)|^2 \mathrm{d}\Omega = \frac{1}{2}\sum_{m=-M}^{M}\frac{1}{h_m^2}\left[k_m^2|\hat{v}_m|^2 + |\hat{\eta}_m|^2\right], \tag{2.11}$$

where $\Omega := [0, 2\pi/k_x] \times [0, 2\pi] \times [0, 2\pi/k_z]$ and V_Ω is the volume of Ω. In this paper we define the 'optimal gain' as the largest value of $E(T)/E(0)$ over all possible initial

https://doi.org/10.1017/jfm.2025.10571 Published online by Cambridge University Press

conditions

$$G(T, k_x, k_z; \beta, Re) := \max_{\boldsymbol{u}(0)} \frac{E(T, k_x, k_z; \beta, Re)}{E(0, k_x, k_z; \beta, Re)}. \tag{2.12}$$

The 'global optimal gain' will be the result of optimising this quantity over the wavenumbers

$$\mathscr{G}(T; \beta, Re) := \max_{\{k_x, k_z\}} G(T, k_x, k_z; \beta, Re), \tag{2.13}$$

and the 'overall optimal gain' will be the result of optimising this over the time T

$$\mathbb{G}(\beta, Re) := \max_{T} \mathscr{G}(T; \beta, Re). \tag{2.14}$$

2.4. *Parameter choices: buffer layer estimates*

The focus in this study is to consider values for the five physical parameters – T, k_x, k_x, β and Re – appropriate for the buffer layer (e.g. Jimenez 2018; Lozano-Durán *et al.* 2021). Given there is no simple characterisation of the mean flow profile here as it adjusts from the viscous sublayer to the log layer and only order of magnitude estimates are sought, we adopt the empirical log layer representation

$$U^+(y^+) = U/u_\tau \approx \frac{1}{\kappa} \ln y^+ + B, \tag{2.15}$$

(where $y^+ = yu_\tau/\nu$ is the distance from the wall in so-called viscous units, u_τ is the friction velocity at the wall, $\kappa \approx 0.4$ and $B \approx 5$) even in the buffer region. Then at a typical buffer scale of $y^+ = 20$, this gives the local Reynolds number

$$Re_{local} \approx y^+ \left(\frac{1}{\kappa} \ln y^+ + B \right) \approx 250, \tag{2.16}$$

which is large but not very large.

A representative T can be found using the time quoted by Lozano-Durán *et al.* (2021) for the maximum gain seen in numerical computations, which is $t = 0.35h/u_\tau$ (h being the half-channel width) at $Re_\tau := hu_\tau/\nu = 180$ and comparable to the eddy turnover time at the appropriate distance from the wall (Markeviciute & Kerswell 2024). The local shear rate at y^+ using the log layer approximation is $S = \mathrm{d}U/\mathrm{d}y = Re_\tau u_\tau/h \, \mathrm{d}U^+/\mathrm{d}y^+ = Re_\tau u_\tau/(h\kappa y^+)$ which gives a time in our inverse shear rate units of

$$T \sim 0.35 \frac{h}{u_\tau} S = 0.35 \frac{Re_\tau}{\kappa y^+} \approx 8, \tag{2.17}$$

for $y^+ = 20$.

In terms of wavenumbers, we take the initial k_y (cross-shear) wavenumber used to non-dimensionalise the model as $2\pi/y^+$ (i.e. the wavelength is the distance to the wall), so the other non-dimensionalised wavenumbers are $k_z \sim O(y^+/(\lambda_z^+ \approx 100))$ and $k_x \sim O(y^+/(\lambda_x^+ \approx 300))$. Therefore both wavenumbers are $O(0.1\text{–}1)$.

The magnitude of β can be estimated by comparing shear rates. Typical root-mean-square velocities near the wall are $u_{rms} \approx 1$ (in units of u_τ) which can be used to estimate typical streak amplitudes. Comparing the ratio of streak shear to wall-normal shear with the model (2.1) gives

$$\frac{k_z^+ u_{rms}}{1/(\kappa y^+)} \approx \frac{k_z \beta/\sqrt{2}}{1}, \tag{2.18}$$

https://doi.org/10.1017/jfm.2025.10571 Published online by Cambridge University Press

or $\beta \approx 3.6$ at $y^+ = 20$ (the $\sqrt{2}$ factor compensates for the cosine dependence in (2.1)). Given this, we consider values of β from 1 to 5 in the below (going to higher β causes problems with numerical overflow in our model: see figure 9).

3. Unbounded constantshear flow ($\beta = 0$): Kelvin's problem

Removing the streaks ($\beta = 0$) recovers Kelvin's classical unbounded constant-shear model (Kelvin 1887) which ever since has proved a popular testing ground for ideas (e.g. Orr 1907; Moffatt 1967; Craik & Criminale 1986; Farrell & Ioannou 1993; Jimenez 2013; Jiao *et al.* 2021). The evolution equations are simply

$$(k^2\hat{v})_t = -\frac{k^2}{Re}(k^2\hat{v}), \qquad \hat{\eta}_t = -\frac{k^2}{Re}\hat{\eta} - \mathrm{i}k_z\hat{v}, \tag{3.1}$$

with the solution

$$\hat{v}(t) = \frac{k^2(0)}{k^2(t)}\hat{v}(0)\mathrm{e}^{\phi(t)}, \qquad \hat{\eta}(t) = \left\{\frac{-\mathrm{i}k_z k^2(0)\hat{v}(0)}{k_x h}\,[\theta(t) - \theta(0)] + \hat{\eta}(0)\right\}\mathrm{e}^{\phi(t)}, \tag{3.2}$$

where

$$\phi(t) := -\frac{1}{Re}\int_0^t k^2(\tau)\,\mathrm{d}\tau, \quad \text{and} \quad \theta(t) := \tan^{-1}\left[\frac{h}{1 - k_x t}\right]; \tag{3.3}$$

(Farrell & Ioannou 1993; Jiao *et al.* 2021). It is well known that two growth mechanisms are present which are revealed by taking the appropriate two-dimensional special case: $k_z = 0$ possesses the Orr mechanism (Orr 1907) only and $k_x = 0$ possesses the lift-up mechanism (Ellingsen & Palm 1975) only.

3.1. *Orr mechanism*

With $k_z = 0$, the shearwise vorticity can only exponentially decay leaving the shrinking of $k^2(t) := k_x^2 + (1 - k_x t)^2$ with time in the expression for $\hat{v}(t)$ – see (3.2) – the sole growth mechanism. Growth occurs for $t \leqslant 1/k_x$ with the viscous (exponential) damping term moderating this. The fact that the growth time does not scale with viscosity means the Orr mechanism is inertial and so considered 'fast'.

For large Re and $1 \lesssim T = o(Re)$, the viscous damping can be ignored and then $k_x = (1/2)(\sqrt{T^2 + 4} - T)$ maximises the global optimal growth at

$$\mathscr{G}^{Orr} = 1/k_x^2 \sim T^2, \tag{3.4}$$

for $T^2 \gg 4$. For $1 \ll T = O(Re)$, the optimal wavenumber is still related to the time via $k_x = 1/T$ to leading order and it is simple to show that the overall growth maximum over T (the overall global optimal) is

$$\mathbb{G}^{Orr} = \frac{9}{\mathrm{e}^2}Re^2, \quad T^{Orr} = 3Re, \quad k_x^{Orr} = \frac{1}{3Re}, \tag{3.5}$$

where $\mathrm{e} = \exp(1) = 2.7183$. So, somewhat paradoxically, the maximum growth over all times produced by the 'fast' Orr mechanism actually occurs on a 'slow' viscous time scale.

3.2. *Lift-up mechanism*

With $k_x = 0$, there is no growth possible in $\hat{v}$ but this velocity component forces the shearwise vorticity $\hat{\eta}$ which grows. This growth ultimately is turned off by the viscous

https://doi.org/10.1017/jfm.2025.10571 Published online by Cambridge University Press

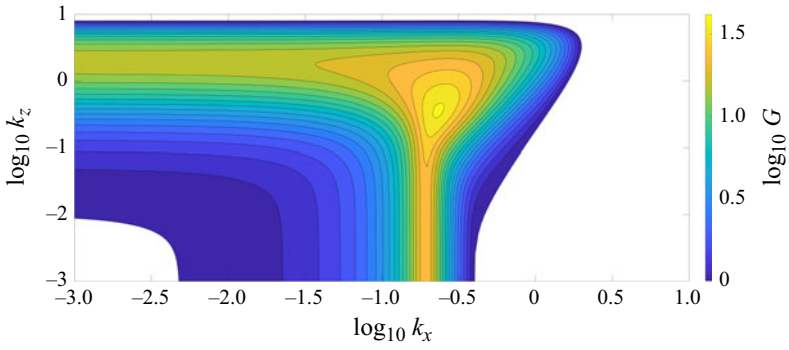

Figure 2. A contour plot of optimal growth G in wavenumber space for $T = 5$ and $Re = 200$. This figure shows that the optimal early time gain occurs for a three-dimensional perturbation, at a location in wavenumber space close to the k_x value associated with the maximum gain possible through the Orr mechanism.

decay of $\hat{v}$ and so lift-up is viewed as a 'slow' viscous process. The overall optimal lift-up growth ($k_x = 0$) is

$$\mathbb{G}^{lift\text{-}up} = \frac{4}{27e^2}Re^2, \quad T^{lift\text{-}up} = \frac{2}{3}Re, \quad k_z^{lift\text{-}up} = \frac{1}{\sqrt{2}}, \tag{3.6}$$

which is consistent with this. Here, since $1 \ll T = O(Re)$, the initial shearwise vorticity can be ignored facilitating the derivation of (3.6) while for $1 \lesssim T = o(Re)$, this is no longer valid.

3.3. *Fully 3-D optimals*

Figure 2 shows the growth landscape over (k_x, k_z) plane for $T = 5$ and $Re = 200$. The optimal k_x wavenumber is close to the (2-D) Orr optimal value ($k_z \to 0$ on the plot) but the optimal k_z is an order of magnitude smaller than the corresponding lift-up value ($k_x \to 0$). This observation is robust over different T as shown in figure 3(*b*) and becomes more exaggerated as T increases towards the maximum at $T = O(Re)$. It is also noticeable in 3(*a*) that this overall optimal gain $\mathbb{G}$ (maximised over all k_x, k_z and T) occurs at about the same time as the Orr maximum (this is clearly not true for lift-up). This and the k_x observation suggests using the large Re results in (3.5) for Orr as a starting point for analysing the full 3-D optimal. Assuming that the initial shearwise vorticity is zero, this leads to

$$\mathbb{G}^{3D} = \frac{9\pi^2}{e^2}Re^2, \quad T^{3D} = 3Re + \alpha Re^{9/11}, \quad k_x^{3D} = \frac{1}{3Re}, \quad k_z^{3D} = \gamma Re^{-8/11}, \tag{3.7}$$

where $\alpha := 3^{6/11}/\pi^{2/11} \approx 1.4786$ and $\gamma := \pi^{3/11}/3^{9/11} \approx 0.5562$. These asymptotic predictions match the numerical computations very well even down to $Re = O(30)$ – see figure 4, also providing *a posteriori* justification for assuming the optimal has $\hat{\eta}(0) = 0$. The formulae in (3.7) give optimal wavenumbers at $Re = 100$ of $(k_x, k_z) = (3.33, 19.53) \times 10^{-3}$ which are consistent with figure 1(*a*) of Jiao *et al.* (2021).

4. Early time transient growth in streaky flow ($\beta \neq 0$)

We now shift our focus to streaky unbounded constant-shear flow and the transient growth possible over $O(1)$ times as discussed in § 2.4. The required optimals will prove to be fully three-dimensional but we start by looking at the reduced two-dimensional (streamwise-independent $k_x = 0$) problem which isolates the unfamiliar 'push-over' mechanism.

https://doi.org/10.1017/jfm.2025.10571 Published online by Cambridge University Press

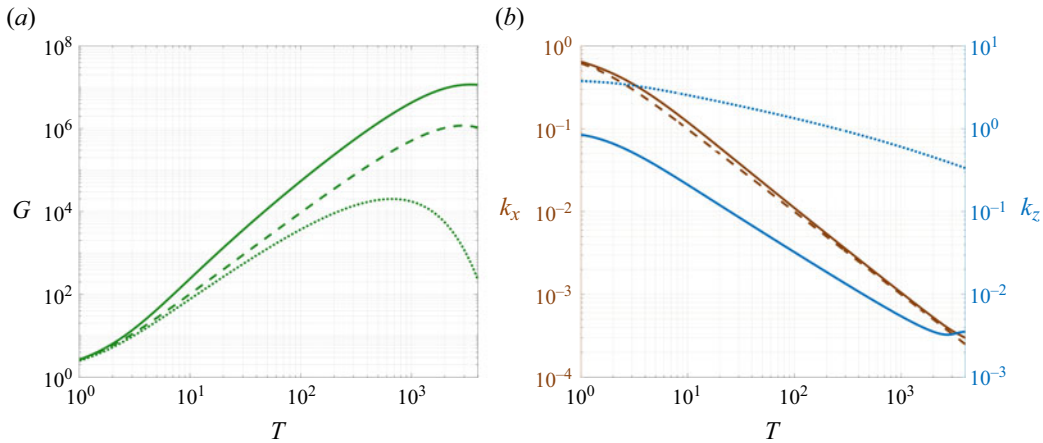

Figure 3. (*a*) optimal growth vs T at $Re = 1000$. The solid line is the full 3-D optimal $\mathscr{G}(Re) = \max_{(k_x,k_z)} G(k_x, k_z; Re)$, the dashed line is $\max_{k_x} G(k_x, 0; Re)$ (Orr) and the dotted line is $\max_{k_z} G(0, k_z; Re)$ (lift-up). (*b*) the corresponding optimal wavenumbers: solid brown/blue for k_x/k_z for the full 3-D optimal, dashed brown for k_x in Orr and dotted blue for k_z in lift up. These plots show that the 3-D optimal closely follows the Orr result in terms of both G and k_x with assistance from lift-up except near the maximum over T (the overall optimal gain $\mathbb{G}$).

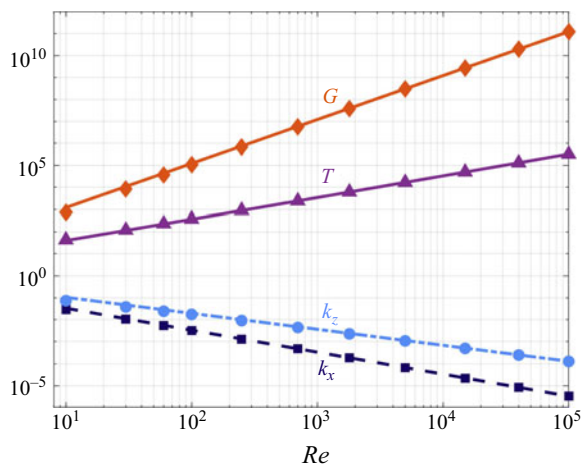

Figure 4. This plot shows the overall optimal gain $\mathbb{G}(\beta, Re)$ and associated optimising parameters (k_x, k_z and T) as a function of Re for $\beta = 0$ in symbols. The asymptotic predictions of (3.7) are the lines.

4.1. *Two dimensional ($k_x = 0$) push-over growth*

With $k_x = 0$, the wavenumbers are constant so Orr is absent and it is simpler to work with the velocity field directly. The $\hat{v}$ and $\hat{w}$ momentum equations together with continuity imply $\hat{p}_m = 0$ for all m, leaving the 3 evolution equations

$$\dot{\hat{u}}_m = -\frac{k_m^2}{Re}\hat{u}_m - \hat{v}_m + \frac{\mathrm{i}\beta k_z}{2}(\hat{w}_{m+1} - \hat{w}_{m-1}), \tag{4.1}$$

$$\dot{\hat{v}}_m = -\frac{k_m^2}{Re}\hat{v}_m, \qquad \dot{\hat{w}}_m = -\frac{k_m^2}{Re}\hat{w}_m, \tag{4.2}$$

https://doi.org/10.1017/jfm.2025.10571 Published online by Cambridge University Press

where $k_m^2 = 1 + m^2 k_z^2$. These indicate that $\hat{v}_m$ and $\hat{w}_m$ simply viscously decay in time allowing explicit solutions to be written down as follows:

$$\hat{u}_m = \mathrm{e}^{-k_m^2 t/Re} \left\{ U_m - V_m t + \frac{\mathrm{i}Re\beta}{2k_z} \left[\frac{W_{m-1}}{1-2m} \left(\mathrm{e}^{-(1-2m)k_z^2 t/Re} - 1 \right) - \frac{W_{m+1}}{1+2m} \left(\mathrm{e}^{-(1+2m)k_z^2 t/Re} - 1 \right) \right] \right\}, \tag{4.3}$$

$$\hat{v}_m = V_m \mathrm{e}^{-k_m^2 t/Re}, \qquad \hat{w}_m = W_m \mathrm{e}^{-k_m^2 t/Re}, \tag{4.4}$$

where $U_m := \hat{u}_m(0)$, $V_m := \hat{v}_m(0)$ and $W_m := \hat{w}_m(0)$ are the initial conditions which, by continuity, satisfy $V_m + mk_z W_m = 0$. Taking $Re \to \infty$ gives the simple $\hat{u}$ equation

$$\hat{u}_m = U_m - V_m t + \frac{\mathrm{i}\beta k_z t}{2} (W_{m+1} - W_{m-1}). \tag{4.5}$$

The push-over effect is produced by the forcing term proportional to the spanwise streak shear, βk_z, and is very similar to the $-V_m t$ lift-up forcing (normalised to have unit shear) although push over drives neighbouring spanwise modes while lift-up is direct. Lift-up can be turned off by setting $V_m = 0$ for $\forall m$ which, through continuity, forces $W_m = 0$ for $m \neq 0$. Setting $U_m = 0$ for all m as well appears an extreme choice for initial conditions but numerical computations indicate that it is close to optimal for $k_x = 0$ (e.g. at $\beta = 1$, $T = 5$ and $Re = 200$, the error using the extreme choice is only $\approx 1\%$ of the global optimal gain value). When only W_0 of the initial conditions is non-zero, the gain is

$$\hat{G}^{push} = \mathrm{e}^{-2T/Re} \left[1 + \frac{Re^2\beta^2}{2k_z^2} \left(1 - \mathrm{e}^{-Tk_z^2/Re} \right)^2 \right] \sim 1 + \frac{1}{2}\beta^2 k_z^2 T^2 \quad \text{as } Re \to \infty, \tag{4.6}$$

assuming $T \ll Re$ and $k_z^2 \ll Re/T$ for the asymptotic simplification (we use a $\hat{}$ to indicate a quantity not optimised over all initial conditions). This mirrors the result for lift-up: when $\beta = 0$ is used, choosing only $(U_1, V_1, W_1) = (0, 1, -1/k_z)$ to be non-zero gives a gain of

$$\hat{G}^{lift\text{-}up} \sim 1 + k_z^2 T^2 / \left(1 + k_z^2 \right), \tag{4.7}$$

at large Re. Hence push over seems to behave very much like lift-up in both the growth possible and the time scales, i.e. growth is ultimately limited by the viscous decay of the spanwise velocities so push over is 'slow'.

The overall optimal gain in (4.6) can be found by optimising over both k_z and T: $\partial \hat{G}^{push}/\partial k_z = \partial \hat{G}^{push}/\partial T = 0$ requires

$$2k_z^2 T e^{-k_z^2 T/Re} - Re \left(1 - \mathrm{e}^{-k_z^2 T/Re} \right) = 0, \tag{4.8}$$

$$Re^2 \beta^2 \left(1 - \mathrm{e}^{-k_z^2 T/Re} \right) \left[\mathrm{e}^{-k_z^2 T/Re} \left(1 + k_z^2 \right) - 1 \right] = 2k_z^2. \tag{4.9}$$

The first of these is solved by noticing that the equation reduces to $2\zeta + 1 - \mathrm{e}^{\zeta} = 0$ with $\zeta := k_z^2 T/Re$ which has the unique positive solution $\zeta \approx 1.256$. Then, using $\mathrm{e}^{-\zeta} = (1 + 2\zeta)^{-1}$ in (4.9) gives the optimal wavenumber as $\hat{k}_z^{push} = \sqrt{2\zeta}$, and thus the maximising time and maximal gain for only-non-vanishing-W_0 initial conditions as

$$\hat{T}^{push} = \tfrac{1}{2} Re \quad \text{and} \quad \hat{\mathbb{G}}^{push} = \frac{\zeta \beta^2}{\mathrm{e}(1 + 2\zeta)^2} Re^2. \tag{4.10}$$

https://doi.org/10.1017/jfm.2025.10571 Published online by Cambridge University Press

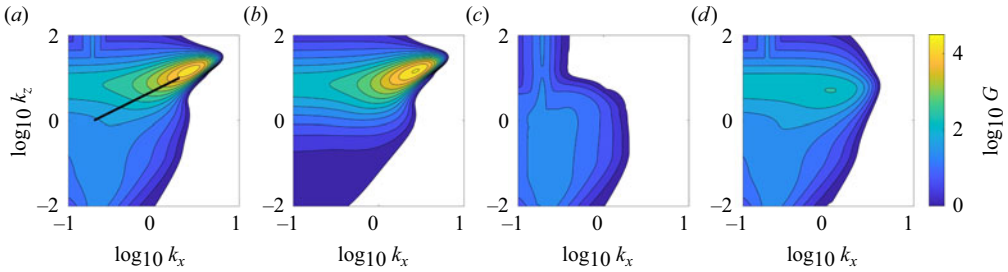

Figure 5. Contour plots of the optimal gain over the (k_x, k_z) wavenumber plane for the parameter set $\beta = 1$, $T = 5$ and $Re = 200$. The truncation value is set to $M = 20$ and the contour levels are the same across all the plots. Panel (*a*) shows the full problem (all terms included), while panels (*b*), (*c*) and (*d*) have the lift-up, push-over and Orr mechanisms removed, respectively. The black line traces the wavenumber ranges used for figure 7. The point of this figure is to show that the large growth observed is substantially suppressed when either the push-over or Orr mechanism is removed, but is largely independent of the lift-up mechanism.

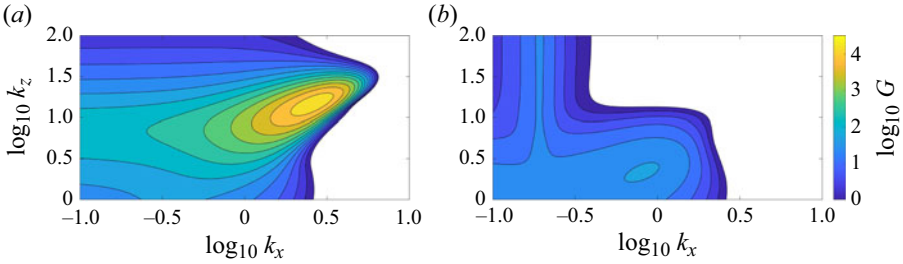

Figure 6. Contour plots of the optimal gain over the (k_x, k_z) wavenumber plane for $\beta = 1$, $T = 5$ and $Re = 200$. Both use $M = 20$ in the model, but the first plots the optimal 'sinuous' disturbances, while the second plots the optimal 'varicose' disturbances (recall that this terminology refers to the symmetry or antisymmetry of u about $z = 0$). This plot demonstrates that all of the large growth occurs for sinuous perturbations.

This again shows that the push-over mechanism, in the absence of Orr ($k_x = 0$) and with initial conditions chosen to eliminate lift-up, possesses the same scalings as the lift-up mechanism.

4.2. *Transient growth of three-dimensional perturbations*

Larger energy growth occurs for 3-D disturbances, where all three mechanisms (lift-up, push over and Orr) can play a role. Figure 5 displays contours of the optimal gain in wavenumber space for four different scenarios at representative parameter values ($\beta = 1$, $T = 5$ and $Re = 200$). The left-most plot shows the gain at T at a given pair of wavenumbers (k_x, k_z) maximised over all initial conditions for the full equations. The other three plots extending to the right have the three growth mechanisms excluded in turn by artificially removing the terms which drive them: figure 5(*b*) has lift-up suppressed by removing $\partial \boldsymbol{U}_B/\partial y$ from the equations; figure 5(*c*) has push over suppressed by removing $\partial \boldsymbol{U}_B/\partial z$; and figure 5(*d*) has the streak advection (the $\beta \cos(k_z z)\partial \boldsymbol{u}/\partial x$ term) removed to suppress the 'spanwise' Orr mechanism (removing all of the advection changes the whole character of the flow). All optimal disturbances here are sinuous with varicose disturbances always producing less growth in this augmented Kelvin model across the parameters considered: e.g. see figure 6.

A key feature of the figure 5(*a*) is the global optimal gain indicated by the yellow region, which reaches values of $\mathscr{G} \approx 10^4$ at $k_x \approx 2.7$ and $k_z \approx 15$. A comparison of this peak and

https://doi.org/10.1017/jfm.2025.10571 Published online by Cambridge University Press

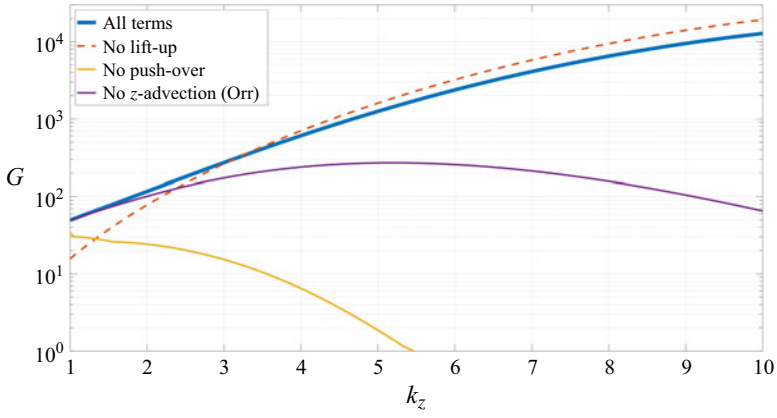

Figure 7. A plot showing the optimal gain as k_z is varied, with $k_x = k_z/5$ and parameters $\beta = 1$, $T = 5$ and $Re = 200$. The range of k_z used here is indicated in figure 5(a) using a black line. The blue line represents the gain when all terms are included in the equations (corresponding the the contours in figure 5(a)). The red line shows the gain when the lift-up mechanism is removed, while the yellow line shows gain when the push-over mechanism is removed and the purple line shows gain when the spanwise Orr mechanism is removed (which correspond to the contours in figures 5(b), 5(c) and 5(d), respectively). This plot demonstrates that both the push-over and spanwise Orr mechanisms are crucial for large growth of kinetic energy, even down to some moderate wavenumbers. It also shows that for smaller wavenumbers, a switch occurs and lift-up becomes the dominant growth process.

the surrounding region with the same location in the other plots reveals that removing the lift-up mechanism leaves the optimal gain contours almost completely unaltered, while removing either the push-over or spanwise Orr mechanism reduces the size of gain significantly. This importance of push over and lack of importance of lift-up for a streaky base flow is fully consistent with earlier observations (Lozano-Durán *et al.* 2021; Markeviciute & Kerswell 2024).

The optimal wavenumbers for this global optimal are, however, on the large side for the buffer layer (see § 2.4) but a line drawn along the major axis of the contours – approximately $k_z = 5k_x$ – suggests a direction of 'shallowest' descent in the wavenumber plane (shown as a black line in figure 5(a) for $1 < k_z < 10$). Figure 7 shows how the optimal gain behaves along this line for $1 < k_z < 10$ when the various mechanisms are excluded. At $k_z = 1$, removing lift-up is actually more detrimental to the gain than removing either spanwise Orr or push over, but for $k_z \gtrsim 3$, the situation is reversed and mimics that for the global optimal gain. The figure also shows that the presence of lift-up now actually hinders growth (the crossing of blue and red lines at $k_z \approx 3$). This effect is also present in figure 5(b) and is consistent with the observations of Lozano-Durán *et al.* (2021) and figure 7 in Markeviciute & Kerswell (2024).

So, the conclusion is, in this unbounded streaky shear flow at these parameters, wavenumber pairings reaching down to those appropriate for buffer-layer dynamics show the clear symbiosis of Orr and push-over mechanisms and the unimportance of lift-up as highlighted by the global optimal gain pairing.

4.3. *A two-variable model of the push-over and Orr interaction*

Remarkably, it is possible to strip the model down to just 2 fields and still retain the symbiotic interaction between push over and Orr. There are 3 distinct steps which achieve this. Firstly, the spanwise truncation M is reduced down to 1 decreasing the number of (complex-valued) fields from $2(2M + 1)$ (with $M = 20$ or so) down to 6. Secondly, the

https://doi.org/10.1017/jfm.2025.10571 Published online by Cambridge University Press

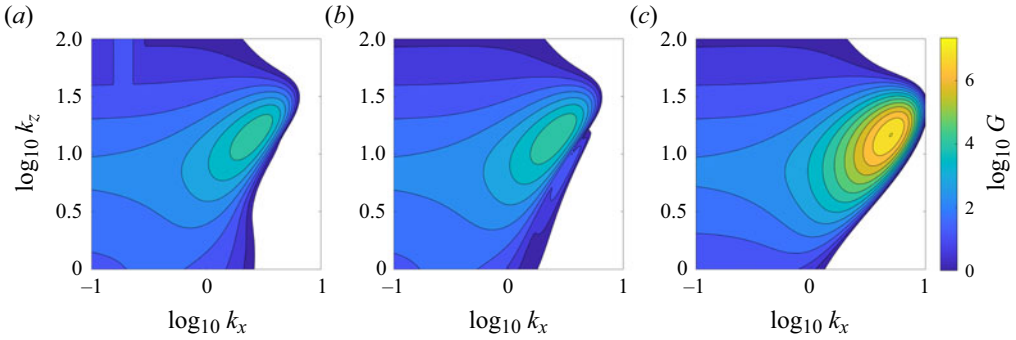

Figure 8. A sequence of contour plots showing the optimal gain in wavenumber space, close to the optimal pair, for the parameter set $\beta = 1$, $T = 5$ and $Re = 200$. The colour bar is shown on the right-hand side and is the same for all three plots. Panel (*a*) has truncation value $M = 20$, (*b*) has $M = 1$ with the sinuous symmetry used and (*c*) uses the further simplification of having $\hat{v}_1$ removed. This figure demonstrates that the underlying growth process is present in all three cases with the reduced model harbouring significantly enhanced growth.

symmetry: $\hat{v}_0 = 0$, $\hat{v}_1 = -\hat{v}_{-1}$ and $\hat{\eta}_1 = \hat{\eta}_{-1}$ appropriate for the sinuous mode (discussed in Schoppa & Hussain 2002) is imposed so 6 becomes 3 complex fields. These evolve as follows:

$$\frac{\mathrm{d}\hat{v}_1}{\mathrm{d}t} = -\frac{k_1^2}{Re}\hat{v}_1 + \frac{2k_x(1-k_xt)}{k_1^2}\hat{v}_1 - \frac{\beta k_z(1-k_xt)}{k_1^2}\hat{\eta}_0, \tag{4.11}$$

$$\frac{\mathrm{d}\hat{\eta}_0}{\mathrm{d}t} = -\frac{k_0^2}{Re}\hat{\eta}_0 - \overbrace{\mathrm{i}\beta k_x\hat{\eta}_1}^{\text{Orr}} + \overbrace{\frac{\beta k_x^2 k_z(1-k_xt)}{h_1^2}\hat{v}_1}^{\text{Orr}} + \overbrace{\frac{\mathrm{i}\beta k_x k_z^2}{h_1^2}\hat{\eta}_1}^{\text{Orr}}, \tag{4.12}$$

$$\frac{\mathrm{d}\hat{\eta}_1}{\mathrm{d}t} = -\frac{k_1^2}{Re}\hat{\eta}_1 - \underbrace{\frac{1}{2}\mathrm{i}\beta k_x\hat{\eta}_0}_{\text{Orr}} - \underbrace{\mathrm{i}k_z\hat{v}_1}_{\text{lift up}} + \underbrace{\frac{\mathrm{i}\beta k_z^2}{2k_x}\hat{\eta}_0}_{\text{push over}}, \tag{4.13}$$

where, recall, $k_0^2 := k_x^2 + (1-k_xt)^2$, $k_1^2 := k_0^2 + k_z^2$ and $h_1^2 := k_x^2 + k_z^2$. Here the Orr, lift-up and push-over terms are labelled in the last two equations and the Orr terms only rely on the streak flow (indicated by being premultiplied by β). The fact that the term involving $\hat{v}_1$ in (4.12) is only an Orr term, and that (4.12) contains no push-over contributions is not obvious; see the Appendix for details.

Finally, $\hat{v}_1$ can be jettisoned meaning (4.11) is ignored and $\hat{v}_1$ set to zero in the $\hat{\eta}$ equations, leaving simply

$$\frac{\mathrm{d}\hat{\eta}_0}{\mathrm{d}t} = -\frac{k_0^2}{Re}\hat{\eta}_0 - \overbrace{\frac{\mathrm{i}\beta k_x^3}{k_x^2+k_z^2}}^{\text{Orr}}\hat{\eta}_1, \tag{4.14}$$

$$\frac{\mathrm{d}\hat{\eta}_1}{\mathrm{d}t} = -\frac{k_1^2}{Re}\hat{\eta}_1 + \frac{1}{2}\mathrm{i}\beta k_x\left[\underbrace{\frac{k_z^2}{k_x^2}}_{\text{push over}}\underbrace{-1}_{\text{Orr}}\right]\hat{\eta}_0. \tag{4.15}$$

https://doi.org/10.1017/jfm.2025.10571 Published online by Cambridge University Press

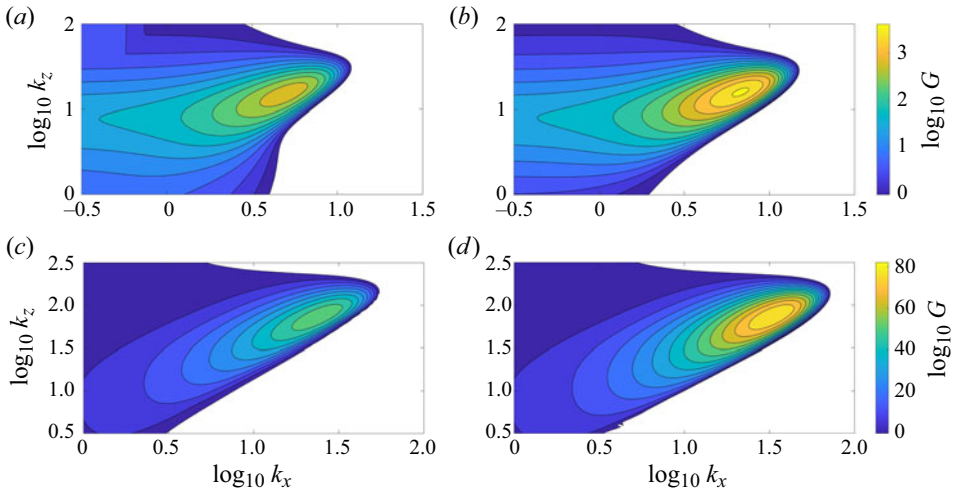

Figure 9. Contour plots in wavenumber space of the optimal gain for $\beta = 1$ (*a*,*b*) and $\beta = 5$ (*c*,*d*), with other parameters set to $T = 2$, $Re = 100$. The first column shows the full model with truncation $M = 20$ while the second column shows the reduced two-variable model given by (4.14) and (4.15).

The *a posteriori* justification for such a drastic reduction is provided by figure 8 which shows the gain in the full ($M = 20$) system (the same data as figure 5(*a*) but replotted over a smaller wavenumber area and with different contour levels), the gain produced by the three-variable model (4.11)–(4.13), and the reduced model (4.14)–(4.15). This comparison clearly shows that: (i) the $M = 1$ reduction is surprisingly effective in retaining the gain behaviour and (ii) the reduced model also retains the global optimal gain feature and in fact, as also observed, experiences significantly enhanced growth with lift-up removed. Figure 9 shows this picture is repeated for smaller $Re = 100$ and target time of $T = 2$ but a larger $\beta = 5$ value (note the increase in contour scale for $\beta = 5$ compared with $\beta = 1$ which is explained by the scaling in (4.27)).

For $Tk_1^2 \ll Re$, diffusion can be dropped in (4.14)–(4.15) and then setting $\hat{\eta}_0 = \eta_0$ and $\hat{\eta}_1 = i\eta_1$ for convenience gives just

$$\frac{\mathrm{d}}{\mathrm{d}t}\begin{pmatrix}\eta_0\\ \eta_1\end{pmatrix} = \begin{pmatrix} 0 & \beta k_x^3/\left(k_x^2+k_z^2\right)\\ \frac{1}{2}\beta\left(k_z^2-k_x^2\right)/k_x & 0\end{pmatrix}\begin{pmatrix}\eta_0\\ \eta_1\end{pmatrix}. \tag{4.16}$$

To arrange for the Euclidean norm to correspond to the energy, the vorticities need to be rescaled – $\tilde{\eta}_0 := \eta_0/h_0$ and $\tilde{\eta}_1 := \sqrt{2}\eta_1/h_1$ – so that

$$E := \frac{1}{2}\left(|\hat{\eta}_0/h_0|^2 + 2|\hat{\eta}_1/h_1|^2\right) = \frac{1}{2}\left(|\tilde{\eta}_0|^2 + |\tilde{\eta}_1|^2\right), \tag{4.17}$$

and the system becomes

$$\frac{\mathrm{d}}{\mathrm{d}t}\begin{pmatrix}\tilde{\eta}_0\\ \tilde{\eta}_1\end{pmatrix} = \mathbb{L}\begin{pmatrix}\tilde{\eta}_0\\ \tilde{\eta}_1\end{pmatrix} := \begin{pmatrix}0 & a\\ b & 0\end{pmatrix}\begin{pmatrix}\tilde{\eta}_0\\ \tilde{\eta}_1\end{pmatrix}, \tag{4.18}$$

where

$$a := \frac{\beta k_x^3}{k_x^2+k_z^2}\frac{h_1}{h_0\sqrt{2}} = \frac{\beta k_x^2}{\sqrt{2\left(k_x^2+k_z^2\right)}}, \qquad b := \frac{\beta\left(k_z^2-k_x^2\right)}{2k_x}\frac{h_0\sqrt{2}}{h_1} = \frac{\beta\left(k_z^2-k_x^2\right)}{\sqrt{2\left(k_x^2+k_z^2\right)}}. \tag{4.19}$$

This system can produce energy growth in 2 distinct and independent ways.

https://doi.org/10.1017/jfm.2025.10571 Published online by Cambridge University Press

(i) Algebraic growth due to the non-normality of $\mathbb{L}$. This occurs when the magnitudes of the off diagonal elements of $\mathbb{L}$ do not match i.e.

$$\frac{a^2}{b^2} = \left(\frac{k_x^2}{k_z^2 - k_x^2}\right)^2 \neq 1 \Rightarrow k_z \neq \sqrt{2}k_x, \tag{4.20}$$

which ensures $\mathbb{L}\mathbb{L}^T \neq \mathbb{L}^T\mathbb{L}$ - the defining property that $\mathbb{L}$ is a non-normal matrix.

(ii) Exponential growth due to a linear instability with growth rate σ where

$$\sigma^2 := ab = \frac{1}{2}\beta^2 k_x^2 \left(\frac{k_z^2 - k_x^2}{k_z^2 + k_x^2}\right). \tag{4.21}$$

This needs $k_z > k_x$ and so push over dominates streak Orr in (4.15). Since only streak Orr operates in (4.14), this clearly shows that push over and streak Orr are needed for this linear instability.

4.4. *Two-variable energy growth*

Either mechanism can act in isolation or together depending on the wavenumber pair (k_x, k_z). In the model studied here, the wavenumbers k_x and k_z are naturally chosen so that both mechanisms are operative as this creates the largest growth. In particular, in the example plotted in figure 8 – $(Re, T, \beta) = (200, 5, 1)$ – the optimal wavenumbers are $(k_x, k_z) \approx (2.7, 15)$ for the $M = 20$ and $M = 1$ models so that $a \approx 0.34$ and $b \approx 10.1$. Hence, $k_z > k_x$ and there is actually a significant difference in magnitude between the off-diagonal elements. To characterise how much energy growth this produces, the 2 differential equations in (4.18) can be straightforwardly integrated to give

$$\begin{pmatrix} \tilde{\eta}_0(t) \\ \tilde{\eta}_1(t) \end{pmatrix} = \mathbb{A}\begin{pmatrix} \tilde{\eta}_0(0) \\ \tilde{\eta}_1(0) \end{pmatrix} := \begin{pmatrix} \cosh\sigma t & \sqrt{a/b}\sinh\sigma t \\ \sqrt{b/a}\sinh\sigma t & \cosh\sigma t \end{pmatrix}\begin{pmatrix} \tilde{\eta}_0(0) \\ \tilde{\eta}_1(0) \end{pmatrix}, \tag{4.22}$$

where $\mathbb{A} = e^{\mathbb{L}t}$. The maximum growth possible, $G(T)$, at $t = T$ for given wavenumbers (k_x, k_z) is then the largest eigenvalue of the real symmetric matrix $\mathbb{A}^T(T)\mathbb{A}(T)$ (here, $\mathbb{A}^T$ indicates the transpose of $\mathbb{A}$ rather than anything to do with the target time T). This is just the larger of the two real positive eigenvalues of the quadratic

$$\lambda^2 - \left[2\cosh^2\sigma T + \left(\frac{a}{b} + \frac{b}{a}\right)\sinh^2\sigma T\right]\lambda + 1 = 0. \tag{4.23}$$

If $\lambda_{max} > 1$ then $\lambda_{min} = 1/\lambda_{max} < 1$, that is, there is only one growth mechanism for a given (k_x, k_z) pairing and no growth implies $\lambda_{max} = \lambda_{min} = 1$. Assuming either large σT when $\sigma^2 = ab > 0$ or $|a/b| \neq O(1)$ for $0 > \sigma^2 = -\omega^2$

$$G(T, k_x, k_z; \beta) := \lambda_{max} \approx 2\cosh^2\sigma T + \left(\frac{a}{b} + \frac{b}{a}\right)\sinh^2\sigma T. \tag{4.24}$$

This shows either linear instability enhanced by initial transient growth as $a/b + b/a \geqslant 2$ or only transient growth in a linearly stable system (ignoring the singular case of $\sin\omega T = 0$). The corresponding optimal condition, which is the associated left eigenvector of $\mathbb{A}^T(T)\mathbb{A}(T)$, depends crucially on whether $a/b \ll 1$ or $\gg 1$. Taking the former and setting $\varepsilon := \sqrt{a/b} \ll 1$ $(k_z/k_x \gg 1)$, the optimal initial condition is

$$\begin{pmatrix} \tilde{\eta}_0(0) \\ \tilde{\eta}_1(0) \end{pmatrix} = \begin{pmatrix} 1 \\ \varepsilon\coth\sigma T \end{pmatrix} \Rightarrow \begin{pmatrix} \tilde{\eta}_0(T) \\ \tilde{\eta}_1(T) \end{pmatrix} = \begin{pmatrix} \cosh\sigma T \\ \frac{1}{\varepsilon}\sinh\sigma T \end{pmatrix}, \tag{4.25}$$

https://doi.org/10.1017/jfm.2025.10571 Published online by Cambridge University Press

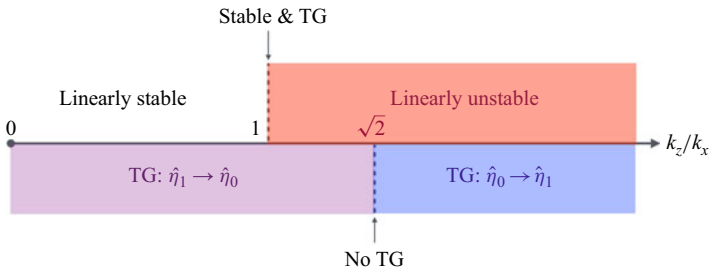

Figure 10. The various transient growth (TG) and stability regimes over $0 \leqslant k_z/k_x$. They are (*a*) $0 \leqslant k_z/k_x < 1$ – linearly stable and $\hat{\eta}_1 \to \hat{\eta}_0$ transient growth; (*b*) $k_z/k_x = 1$ – linearly stable but unlimited algebraic growth in $\hat{\eta}_0$; (*c*) $1 < k_z/k_x < \sqrt{2}$ – linearly unstable and $\hat{\eta}_1 \to \hat{\eta}_0$ transient growth; (*d*) $k_z/k_x = \sqrt{2}$ – linearly unstable with no transient growth; and (*e*) $\sqrt{2} < k_z/k_x$ – linearly unstable and $\hat{\eta}_0 \to \hat{\eta}_1$ transient growth. Sample evolutions are shown for $k_z/k_x = 5.6$ in figure 13 and $k_z/k_x = 0.95$ in figure 14 for $(Re, T, \beta) = (200, 5, 1)$.

along with what it evolves into a time T later (all to leading order in ε). This indicates that energy growth through the non-normality of $\mathbb{L}$ is produced by initial $\hat{\eta}_0$ generating $\hat{\eta}_1$ as described by (4.15). This is consistent with what Schoppa & Hussain (2002) found – the initial condition they chose was purely $\hat{\eta}_0$ – but they focussed on the streamwise vorticity as a measure of the growth rather than the shearwise vorticity.

If instead, $a/b \gg 1$ so now $\varepsilon := \sqrt{b/a} \ll 1$ (or $k_z^2/k_x^2 - 1 \ll 1$), the optimal initial condition is

$$\begin{pmatrix} \tilde{\eta}_0(0) \\ \tilde{\eta}_1(0) \end{pmatrix} = \begin{pmatrix} \varepsilon \coth \sigma T \\ 1 \end{pmatrix} \Rightarrow \begin{pmatrix} \tilde{\eta}_0(T) \\ \tilde{\eta}_1(T) \end{pmatrix} = \begin{pmatrix} \frac{1}{\varepsilon} \sinh \sigma T \\ \cosh \sigma T \end{pmatrix}. \tag{4.26}$$

This indicates that energy growth through the non-normality of $\mathbb{L}$ is now produced by initial $\hat{\eta}_1$ generating $\hat{\eta}_0$ as described by equation (4.14).

Given instability exists for $ab > 0$ or $k_z > k_x$, there are 5 different scenarios as k_z/k_x varies: see figure 10. Optimising energy growth over all wavenumbers should select either $1 < k_z/k_x < \sqrt{2}$ or $\sqrt{2} < k_z/k_x$ since both are linearly unstable but have different transient growth mechanisms. Computations here suggest it is the latter which contains the optimum which is consistent with where the instability growth rate is larger for fixed k_x. In this case, the transient growth which occurs is described by (4.15) and push over is the dominant process. This transient growth situation is illustrated in figure 11(*a*). Here, the spanwise velocity perturbation $\hat{w}_0 := \mathrm{i}\hat{\eta}_0/k_x$ 'pushes over' (advects) the base streak velocity $\beta \cos(k_z z)\,\hat{\boldsymbol{x}}$ to create wavy streaks $\hat{u}_1$ (and so $\hat{\eta}_1$) via the projection of the term $\hat{w}_0 \partial/\partial z U_B$ onto the $\hat{u}_1$ equation. The (streak) Orr achieves the same effect of generating streamwise- and spanwise-dependent flow from only streamwise-dependent flow – albeit with the opposite and wrong phase for subsequent instability.

4.5. *Two-variable linear instability*

The instability looks to be exactly the 2-D linear instability of a streak field as modelled by 2-D Kolmogorov flow (Arnold & Meshalkin 1960; Meshalkin & Sinai 1961). In its simplest form, Kolmogorov flow consists of a steady forcing, $\sin \ell y\,\hat{\boldsymbol{x}}$ for some integer ℓ, applied to a flow over a two-torus $[0, 2\pi/\hat{\alpha}] \times [0, 2\pi]$. The corresponding one-dimensional base flow is exactly the streak flow studied here with the base shear removed and is linearly unstable at high enough Re provided $\hat{\alpha} < \ell$ which is exactly the condition $k_x < k_z$ for instability found in (4.16) (e.g. Marchioro (1986) and figure 2 in Chandler & Kerswell (2013)).

https://doi.org/10.1017/jfm.2025.10571 Published online by Cambridge University Press

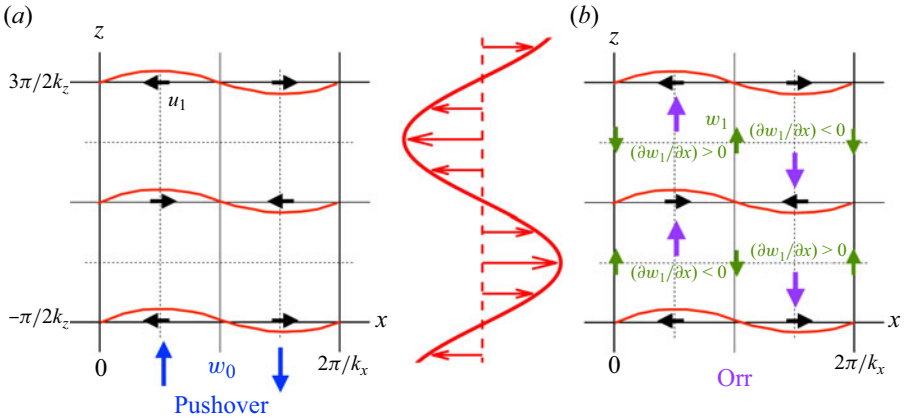

Figure 11. (*a*) $\hat{\eta}_0$ corresponds to a spanwise velocity $w_0 \propto \sin k_x x$ which 'pushes over' the streak velocity field $\beta \cos k_z z\, \hat{\boldsymbol{x}}$ to produce wavy streaks as shown created by the streamwise velocity anomalies $u_1 \propto \sin k_x x \sin k_z z$ (black arrows). (*b*) the spatial gradients in the u_1 field imply a doubly periodic pressure field which drives a concomitant spanwise velocity $w_1 \propto \cos k_x x \cos k_z z$ field (green arrows). The advection of this w_1 field by the streak velocity – the streak-Orr effect – generates further spanwise velocity (purple arrows) via the term $-\beta \cos k_z z \partial w_1/\partial x$ which feeds back positively on $\hat{\eta}_0$ completing the loop.

The instability is produced by a further mechanism represented by (4.14) which generates $\hat{\eta}_0$ from $\hat{\eta}_1$ to complement the transient growth mechanism. As discussed above, the latter produces wavy streaks which drive a concomitant spanwise field $\hat{w}_1$ through continuity ($k_x \neq 0$): see figure 11(*b*). This spanwise field $\hat{w}_1$ then drives $\hat{w}_0$ to close the loop by the streak-Orr mechanism. that is, streak advection of $\hat{w}_1$ given by the projection of the $\beta \cos(k_z z) \mathrm{i} k_x \hat{w}_1$ term onto the $\hat{w}_0$ equation: again see figure 11(*b*). In this process, the streamwise flow component of the instability, $\hat{u}_1$, is largest at the inflexion points of the streak field where the spanwise shear is maximal, while the spanwise flow component is largest when the streak is largest.

4.6. *Two-variable transient growth with dissipation present*

Before studying the nonlinear consequences of the linear instability, we estimate the energy growth possible in the two-variable system with dissipation present. Because of the unlimited growth of the cross-stream wavenumber in the model, dissipation always eventually overpowers the instability to formally give only transient growth. For a general k_x, the time for the cessation of linear instability growth is given by the balance $\beta k_x \sim k_x^2 T^2/Re$ so $T = O(\sqrt{\beta Re/k_x})$ and then a prediction for the optimal growth for a *given* $k_x \lesssim O(Re)$ is

$$G \sim \mathrm{e}^{\sqrt{\alpha \beta^3 k_x Re}}, \tag{4.27}$$

where $\alpha = 1/2(k_z^2 - k_x^2)/(k_z^2 + k_x^2)$ is $O(1)$. Formally, if $T \gtrsim O(1)$, this is maximised for $k_x = O(Re)$ beyond which diffusion dominates giving a massive gain of $O(\mathrm{e}^{\alpha_1 Re})$ (α_1 being a Re-independent number). This prediction is confirmed in the two-variable model and for the full system: see figure 12. This also shows good correspondence between the optimal wavenumbers in each system which all scale linearly with Re. Figure 12 also confirms that a push-over-less system has no such exponential growth. However, this overall optimal gain is not the one of practical interest as $k_z = O(Re)$ (figure 12 actually has $k_z \sim 0.075Re$ and $k_x \sim 0.012Re$) represents unrealistically large streak shear. If, instead $k_z = O(1)$ (and hence $k_x = O(1)$), the gain is reduced but still substantial at $O(\mathrm{e}^{\alpha_2 \sqrt{Re}})$

https://doi.org/10.1017/jfm.2025.10571 Published online by Cambridge University Press

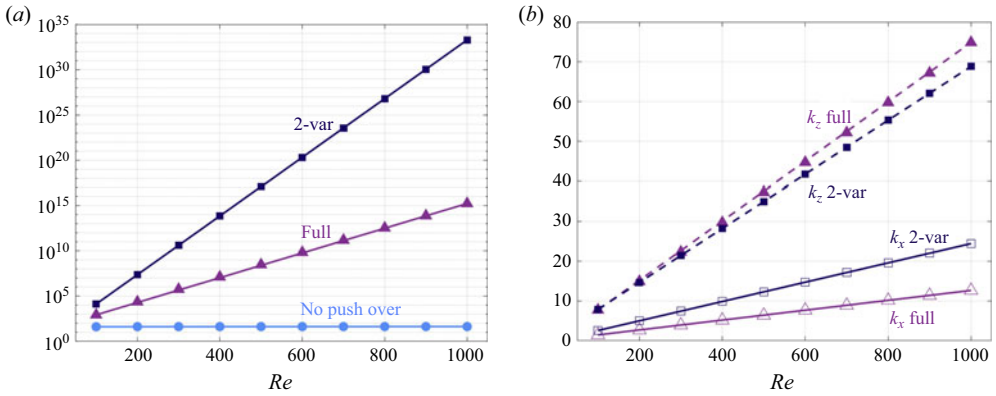

Figure 12. (*a*) plot shows the global optimal gain $\mathscr{G}$ as a function of Re for $\beta = 1$, $T = 5$ using the full ($M = 20$) system (purple triangles), the reduced two-variable model (dark blue squares) and the full system with push over removed (dull blue circles). The lines drawn through the data are the straight lines between the extreme points of each data set indicating that the full system has the same $\mathscr{G} \sim \mathrm{e}^{\alpha Re}$ behaviour as the two-variable model albeit with a smaller α. The push-over-less system does not have this exponential dependence. (*b*) plot compares the optimal wavenumbers between the full system and the reduced two-variable model (the symbols). Lines through the data (drawn as in the Left plot) indicate that all wavenumbers scale linearly with Re.

generated over $O(\sqrt{Re})$ 'intermediate' times (α_2 being another constant). This exponential dependence of gain on $\sqrt{Re}$ is surprising given that the Orr and push-over mechanisms in isolation only give gains which scale like Re^2 and then only over 'slow' times of $O(Re)$ (e.g. see §§ 3 and 4.1).

4.7. *Nonlinear feedback of the two-variable system*

The linear instability in 2-D Kolmogorov flow is known to be supercritical (Sivashinsky 1985) and hence the first nonlinear feedback of the instability on the streak is to reduce its amplitude. As confirmation, the instability here is

$$\boldsymbol{u} = \begin{bmatrix} \frac{2k_z}{h_1^2}\hat{\eta}_1(t)\sin k_z z \\ 0 \\ \frac{2ik_x}{h_1^2}\hat{\eta}_1(t)\cos k_z z + \frac{i}{k_x}\hat{\eta}_0(t) \end{bmatrix} e^{i(k_x x + (1-k_x t)y)} + \text{c.c.}; \tag{4.28}$$

(c.c. indicating complex conjugate) which, indeed, has the negative feedback on the streak

$$\frac{k_x k_z}{2\pi^2}\int_0^{2\pi/k_z}\int_0^{2\pi/k_x}(-\boldsymbol{u}\cdot\nabla u)\cos k_z z\,\mathrm{d}x\mathrm{d}z = -\frac{4k_z^2}{k_x h_1^2}Re\big(i\hat{\eta}_0\hat{\eta}_1^*\big) < 0, \tag{4.29}$$

as $\hat{\eta}_1 = i\hat{\eta}_0\sqrt{k_z^4/k_x^{4-1}}/\sqrt{2}$ from (4.15) ignoring diffusion (* indicates complex conjugate and $Re(\,)$ is the real part). So this two-variable system does not re-energise the imposed streaks and moreover has no feedback on any streamwise rolls. To generate the latter, $\hat{v}_1$ needs to be reinstated – i.e. we need to examine the full three-variable $M = 1$ system – but at a cost of expecting less growth.

4.8. *Three-variable feedback onto rolls*

The $M = 1$ linear system, (4.11)–(4.13) has a symmetry that if $(\hat{\eta}_0, \hat{\eta}_1, \hat{v}_1)$ is a solution then so is $(\hat{\eta}_0^*, -\hat{\eta}_1^*, \hat{v}_1^*)$. This symmetry is adopted by optimal initial conditions so that

https://doi.org/10.1017/jfm.2025.10571 Published online by Cambridge University Press

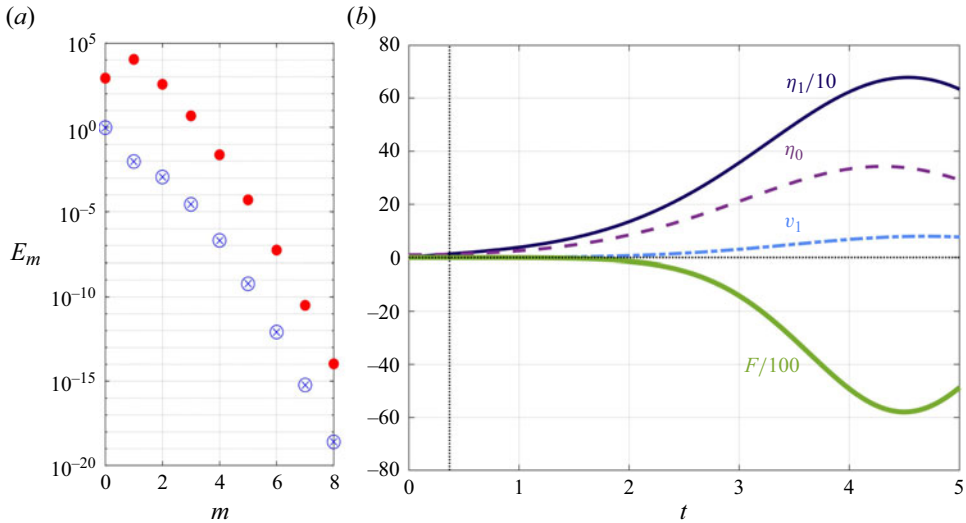

Figure 13. (*a*) modal energy $E_m := (1/2h_m^2)(k_m^2|\hat{v}_m|^2 + |\hat{\eta}_m|^2)$ plotted over $m \geqslant 0$ ($E_{-m} = E_m$ due to symmetry) for the initial optimal (blue circled crosses) and final state (red filled circles) for $(Re, T, \beta) = (200, 5, 1)$ and $M = 20$. This indicates why the $M = 1$ truncation works so well: the initial optimal has its energy dominantly in the $m = 0$ mode which shifts to $m = 1$ by the final state. (*b*), the time evolution of the optimal for $M = 1$ system and $(Re, T, \beta) = (200, 5, 1)$: solid dark blue uppermost line is $\eta_1/10$; dashed purple line is η_0 and the dash-dot pale blue line is v_1. The green solid line indicating negative values is $F/100$ where F is defined in (4.31). The dotted vertical line at $t \approx 0.37$ indicates where $1 - k_x t = 0$ for $k_x \approx 2.7$ and $k_z \approx 15$.

the flow subsequently can then be assumed of the form $(\hat{\eta}_0, \hat{\eta}_1, \hat{v}_1) = (\eta_0(t), i\eta_1(t), v_1(t))$ where $\eta_0(t)$, $\eta_1(t)$ and $v_1(t)$ are all real variables subsequently (this observation has already been used to produce equation (4.16)). The evolution of these 3 optimal real variables is shown in figure 13(*b*) for $(Re, T, \beta) = (200, 5, 1)$. The three-variable flow field takes the form

$$\boldsymbol{u} = \begin{bmatrix} 2i\,\{-k_x(1-k_x t)v_1(t) + k_z\eta_1(t)\}\sin k_z z/h_1^2 \\ 2i\,v_1(t)\sin k_z z \\ 2\,\{-k_z(1-k_x t)v_1(t) - k_x\eta_1(t)\}\cos k_z z/h_1^2 + i\eta_0(t)/k_x \end{bmatrix} e^{i(k_x x + (1-k_x t)y)} + \text{c.c.}, \tag{4.30}$$

and the nonlinear driving of the cross-stream flow component $V(z, y)\hat{\boldsymbol{y}}$ with the same spanwise structure relevant for lift up is

$$F := \frac{k_x k_z}{2\pi^2}\int_0^{2\pi/k_z}\int_0^{2\pi/k_x}(-\boldsymbol{u}\cdot\nabla v)\cos k_z z\,\mathrm{d}x\mathrm{d}z = -\frac{4k_z}{k_x}\eta_0(t)v_1(t). \tag{4.31}$$

For the representative parameters used in figure 13(*b*), $\eta_0 > 0$ and $v_1 > 0$ and so the feedback F is large and negative (note that $F/100$ is actually plotted). This drives secondary cross-stream velocities anti-correlated ($\propto -\cos k_z z$) to the imposed streak field which, through the lift up term $-U_y V\,\hat{\boldsymbol{x}}$ reinforces the existing streak field. Specifically, where the instability generates $V > 0$, slower moving fluid from the basic shear is 'lifted up' to reinforce the slow streaks (where $\beta\cos k_z z < 0$) and where $V < 0$, corresponding faster-moving fluid is 'pushed down' to reinforce the fast streaks (where $\beta\cos k_z z > 0$). Since the driven flow $V(y, z)\hat{\boldsymbol{y}}$ is synonymous with streamwise rolls, this demonstrates the potential for this streak instability to produce a sustaining cycle of rolls and streaks (Hamilton *et al.* 1995; Waleffe 1997; Jimenez & Pinelli 1999; Farrell & Ioannou 2012).

https://doi.org/10.1017/jfm.2025.10571 Published online by Cambridge University Press

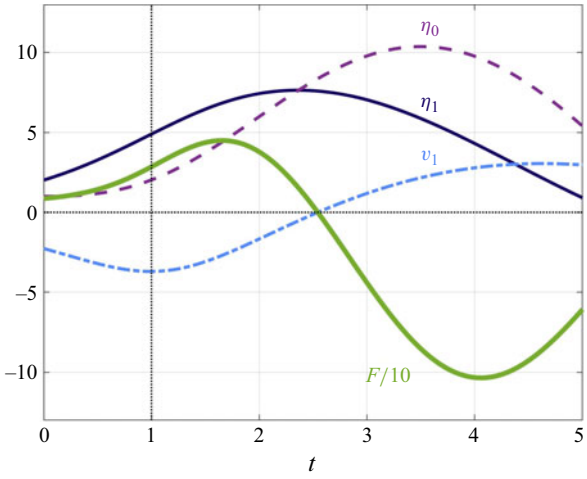

Figure 14. The time evolution of the optimal for $M = 1$ system and $(Re, T, \beta) = (200, 5, 1)$ with non-optimal $k_x = 1$ and $k_z = 0.95$ so a linear stable situation: solid dark blue line is η_1; dashed purple line is η_0 and the dash-dot pale blue line is v_1. The green solid line indicating largely negative values is $F/10$ where F is defined in (4.31). The dotted vertical line indicates when $1 - k_x t = 0$.

Figure 14 confirms for non-optimal wavenumbers – $k_x = 1$ and $k_z = 0.95$ – with no instability present that even the transient growth acting alone provides good nonlinear feedback onto streamwise rolls.

4.9. *Why lift up weakens growth*

Figure 8 shows that removing $\hat{v}_1$ from the $M = 1$ system considerably enhances the optimal growth. This is because both the $\hat{v}_1$-Orr term in (4.12) and the lift-up term in (4.13) weaken the instability mechanism which dominates the growth found here. Starting with figure 11(*a*) or (4.13), the presence of the lift-up term works against the push-over effect of $\hat{\eta}_0$. The x- and z-phases of $\hat{v}_1$ are the same as that for $\hat{u}_1$ created by $\hat{\eta}_0$ (see (4.30)) so $\hat{v}_1$ is either lifting up or pushing down the base shear flow to reduce the magnitude of $\hat{u}_1$. By this same reasoning, lift up can enhance the transient growth process if Orr dominates push over – i.e. there is no instability – but this scenario is never selected when maximising growth over wavenumber space.

In figure 11(*b*), the possibility of motion into or out of the x-z plane of the streaks reduces the spanwise flow field $\hat{w}_1$ generated by the $\hat{u}_1$ field through continuity (the pressure field associated with the spatial gradients of $\hat{u}_1$ now can drive both $\hat{v}_1$ and $\hat{w}_1$ fields rather than just $\hat{w}_1$). This reduced $\hat{w}_1$ then has weakened spatial gradients and so diminishes the streak-Orr effect. In terms of (4.12), this manifests itself as the $\hat{v}_1$-Orr term acting against the $\hat{\eta}_1$-Orr terms once $(1 - k_x t) < 0$ which happens early in the evolution (e.g. see figure 13(*b*)).

4.10. *Previous work*

The linear instability isolated here in (4.16) is inviscid in nature and, at least in terms of the streamwise and cross-stream velocity components, is centred at the spanwise inflexion points of the streaks where the streak shear is maximal. This suggests it is related to the linear instability originally observed by Swearingen & Blackwelder (1987). Against this, the spanwise flow components are maximal at the streak flow extrema, but there are no

https://doi.org/10.1017/jfm.2025.10571 Published online by Cambridge University Press

cross-stream inflexion points in this model and so no Kelvin–Helmholtz type instability (e.g. see figure 19*b* of Kline *et al.* 1967).

The model has revealed two transient growth mechanisms that can be in play for different wavenumber pairings. The one which is selected by optimising over the wavenumbers corresponds to that found originally by Schoppa & Hussain (2002) (e.g. their initial condition is very similar to the optimal conditions found here dominated by $\hat{\eta}_0$). There, the authors concentrated on the growth of the streamwise vorticity (e.g. see their figure 11(*b*) and § 4.2) identifying what they called a 'shearing' generation of vorticity due to the right hand side term in their (14*a*) and illustrated in their figure 16. This is a purely Orr term as there are no lift-up or push-over terms in the streamwise vorticity equation and those authors attributed it predominantly to the base cross-stream shear (see just below (13) in Schoppa & Hussain (2002)). Here, we instead find that push over is the more important mechanism which has to dominate (streak) Orr to see this growth. When this happens, the two-variable inviscid model is also linear unstable, that is, there are no wavenumber pairs for which this transient growth occurs with the flow stable (see figure 10). Plausibly, introducing diffusion which stays bounded rather than growing steadily as here would introduce a threshold for instability so recreating the possibility of a stable, transient growth scenario studied by Schoppa & Hussain (2002).

Finally, it is worth remarking that, for reasons of simplicity, we have identified the Orr mechanism only with advection terms and these don't contribute to the perturbation energy equation. This means that there must be either lift up or push over operating as well to actually get energy growth. The model studied here strongly suggests that push over is the key mechanism which is consistent with the findings of Hoepffner *et al.* (2005): their figure 6(*a*) shows that energy input from the streak field dominates that from the base shear.

5. Discussion

In this paper, motivated by recent numerical experiments on near-wall turbulence by Lozano-Durán *et al.* (2021), we have considered Kelvin's unbounded, constant-shear model augmented by a spatially periodic spanwise shear to include streaks. This addition allows a little-studied transient growth mechanism – push over – to be explored along with its interactions with the more familiar Orr and lift-up mechanisms. Consistent with the findings of Lozano-Durán *et al.* (2021) and subsequent analysis by Markeviciute & Kerswell (2024), this model clearly shows that the Orr and push-over mechanisms can combine to produce considerably enhanced transient growth for streaky base flows over that produced individually, and that lift-up is unimportant, actually tending to reduce peak growth (although, of course, lift-up is believed central for the roll-to-streak regenerative process).

The heart of this symbiotic interaction is laid bare in (4.16) which describes the evolution of a stripped down two-variable version of the model. This shows that for the optimal set of perturbation wavenumbers, there are actually two distinct mechanisms for growth: (i) a transient growth mechanism by which the spanwise-independent but streamwise-periodic cross-stream vorticity $\hat{\eta}_0$ generates spanwise-dependent streamwise-periodic cross-stream vorticity $\hat{\eta}_1$ involving push-over and Orr processes, and (ii) a linear instability mechanism where $\hat{\eta}_1$ reciprocates by generating $\hat{\eta}_0$ via an Orr process in such a way as to give sustained asymptotic growth. Only when push over dominates Orr does the output of the growth – $\hat{\eta}_1$ – have the right spanwise phase to feedback on the input of the growth – $\hat{\eta}_0$ – to produce sustained asymptotic growth. In the model, wavenumbers invariably exist to achieve this and so very large growth occurs.

Reinstating diffusion always eventually overpowers this growth due to the unlimited increase of the cross-shear wavenumber (an unfortunate feature of the model) but, in the

https://doi.org/10.1017/jfm.2025.10571 Published online by Cambridge University Press

meantime, huge growth, scaling like $e^{\alpha_1 Re}$, can occur over 'fast' $T = O(1)$ times. Even restricting the wavenumbers considered to be $O(1)$ appropriate for a turbulent boundary layer can produce growths scaling like $e^{\alpha_2\sqrt{Re}}$ over 'intermediate' $T = O(\sqrt{Re})$ times (with α_1 and α_2 constants). This is in marked contrast to the algebraic growth factors associated with Orr and lift-up, and now also shown here for push over in isolation (see (4.10)), of gain $\sim Re^2$ over 'slow' $T = O(Re)$ times.

Reinstating the presence of a cross-shear velocity $\hat{v}_1$ is found to weaken the instability mechanism in two ways. Firstly, the reinstalled lift-up mechanism hampers the action of push over in the transient growth mechanism. Secondly, there is an antagonistic $\hat{v}_1$-Orr term – third term on the right-hand side of (4.12) – which hinders the generation of $\hat{\eta}_0$. This term grows with the cross-shear wavenumber and eventually curtails the instability completely (and, for the parameters studied, actually before diffusion). The presence of $\hat{v}_1$, however, is crucial in setting up the correct nonlinear feedback to generate the right type of streamwise rolls to re-energise the imposed streaks via lift up. Hence this model indicates the presence of the sustaining cycle in a simple shear flow.

With regards time scales, even just considering Kelvin's original model (no streaks) exposes the oversimplification of labelling mechanisms with one timescale based on what turns it off. Orr is considered 'fast' and lift-up 'slow' yet both give the same levels of growth at $T = O(1)$ – see (3.4) and (4.7) – and their overall optimal gains are both achieved at $T = O(Re)$ and scale similarly with Re^2 – see (3.5) and (3.6). Just to complicate matters, the push-over mechanism behaves exactly equivalently – see (4.6) and (4.10) – so there is no time scale puzzle: they all operate across inertial and viscous times. What perhaps is a surprise is that the relevant Orr mechanism revealed here is based on streak advection rather than the usual basic shear advection.

Of course, the model treated here has its limitations. The streaks have no cross-shear structure (as there are no boundaries although Schoppa & Hussain (2002) comment that this is unimportant for the important sinuous modes – see their p67) so there are no cross-shear inflexion points. There is also the unlimited growth of the shearwise wavenumber so that diffusion eventually overpowers any apparent linear instability. Nevertheless, the model manages to clarify the transient growth mechanism originally found by Schoppa & Hussain (2002) (which is push over dominated), and also indicates how this transient growth is related to the streak instability centred on the spanwise inflexion points observed by Swearingen & Blackwelder (1987) (it forms one half of the loop). Using it, we have also been able to verify that the correct nonlinear feedback occurs onto the right streamwise rolls to re-energise the assumed streaks. Finally, a connection has also been made to the well-known linear instability in 2-D Kolmogorov flow.

Acknowledgements. The authors are very grateful to two referees whose comments helped considerably improve the presentation of this work.

Funding. W.O. acknowledges financial support from EPSRC in the form of a studentship.

Declaration of interests. The authors report no conflict of interest.

Appendix. The Absence of Push Over in the Evolution of z-independent Vorticity

This appendix explains the reason for the absence of any push-over contributions in the evolution equation (4.12) for $\hat{\eta}_0$. This is not a trivial fact when using (2.5) as a starting point as an Orr and a push-over term must be combined using continuity to arrive at the term involving $\partial v/\partial y$. The source of all the terms can be identified more clearly by starting with the original momentum equation given by (2.2) (where the terms associated with each

https://doi.org/10.1017/jfm.2025.10571 Published online by Cambridge University Press

physical mechanism are clear), and advancing towards equations (2.4) and (2.5) without making any simplifications or cancellations. The final two terms in (2.5) are broken down as

$$-\overbrace{\beta k_z \sin(k_z z)\frac{\partial u}{\partial x}}^{\text{Orr}} - \overbrace{\beta k_z \sin(k_z z)\frac{\partial w}{\partial z}}^{\text{Push}} - \overbrace{\beta w k_z^2 \cos(k_z z)}^{\text{Push}}, \tag{A1}$$

where the push-over contributions shown here are, in fact, the only push-over terms present in the evolution equation for η (the advection term in (2.5) is associated with Orr while the $\partial v/\partial z$ term is associated with lift-up).

To proceed towards equation (4.12), the Kelvin modes in (2.7) are used with $M = 1$ along with the sinuous symmetry property discussed in § 4.3. The variables can be written in a reduced manner, in particular $w = [\hat{w}_0 + 2\cos(k_z z)\hat{w}_1]\mathrm{e}^{\mathrm{i}[k_x x + (1-k_x t)y]}$. The terms labelled as push over in (A1) are then simplified to

$$2\beta k_z^2 \sin^2(k_z z)\hat{w}_1 - 2\beta k_z^2 \cos^2(k_z z)\hat{w}_1 - \beta k_z^2 \cos(k_z z)\hat{w}_0, \tag{A2}$$

where the exponential multiplication factor is removed for clarity. The first two terms are merged to produce a quantity involving $\cos(2k_z z)$, which shows that there are no z-independent contributions found from the push-over mechanism; it will not contribute in the evolution equation for the z-independent component of vorticity, $\hat{\eta}_0$. This makes it clear that the $\hat{v}_1$ term in (4.12) (that is subsequently ignored) is only of Orr origin, as is the $\hat{\eta}_1$ term that is retained.

The last term in (A2) also produces the full push-over contribution to the $\hat{\eta}_1$ evolution equation given by (4.13). The identification of Orr and lift-up is then made more simple as any remaining terms will be an Orr contribution if and only if they contain a factor of β.

References

Arnold, V.I. & Meshalkin, L.D. 1960 The seminar of A.N. Kolmogorov on selected topics in analysis (1958–1959). *Usp. Mat. Nauk.* **15**, 247–250.

Bayly, B.J. 1986 Three-dimensional instability of elliptical flow. *Phys. Rev. Lett.* **57**, 2160–2163.

Butler, K.M. & Farrell, B.F. 1993 Optimal perturbations and streak spacing in wall-bounded turbulent shear flow. *Phys. Fluids A* **5** (3), 774–777.

Cassinelli, A., De Giovanetti, M. & Hwang, Y. 2017 Streak instability in near-wall turbulence revisited. *J. Turbul.* **18**, 443–464.

Chandler, G.J. & Kerswell, R.R. 2013 Invariant recurrent solutions embedded in a turbulent two-dimensional Kolmogorov flow. *J. Fluid Mech.* **722**, 554–595.

Craik, A. & Criminale, W. 1986 Evolution of wavelike disturbances in shear flows: a class of exact solutions of the Navier–Stokes equations. *Proc. R. Soc. Lond.* **A406**, 13.

Craik, A.D.D. 1988 A class of exact-solutions in viscous incompressible magnetohydrodynamics. *Proc. R. Soc. A* **417**, 235–244.

Craik, A.D.D. 1989 The stability of unbounded 2-dimensional and 3-dimensional flows subject to body forces - some exact solutions. *J. Fluid Mech.* **198**, 275–292.

Ellingsen, T. & Palm, E. 1975 Stability of linear flow. *Phys. Fluids.* **18** (4), 487–488.

Farrell, B.F. & Ioannou, P.J. 1993 Optimal excitation of three-dimensional perturbations in viscous constant shear flow. *Phys. Fluids A* **5** (6), 1390–1400.

Farrell, B.F. & Ioannou, P.J. 2012 Dynamics of streamwise rolls and streaks in turbulent wall-bounded shear flow. *J. Fluid Mech.* **708**, 149–196.

Hamilton, J.M., Kim, J. & Waleffe, F. 1995 Regeneration mechanisms of near-wall turbulence structures. *J. Fluid Mech.* **287**, 317–348.

Hartman, R.J. 1975 Wave propagation in stratified shear-flow. *J. Fluid Mech.* **71**, 89–104.

Hoepffner, J., Brandt, L. & Henningson, D.S. 2005 Transient growth on boundary layer streaks. *J. Fluid Mech.* **537**, 91–100.

Jiao, Y., Hwang, Y. & Chernyshenko, S.I. 2021 Orr mechanism in transition of parallel shear flow. *Phys. Rev. Fluids* **6** (2), 023902.

https://doi.org/10.1017/jfm.2025.10571 Published online by Cambridge University Press

JIMENEZ, J. 2012 Cascades in wall-bounded turbulence. *Annu. Rev. Fluid Mech.* **44**, 27–45.
JIMENEZ, J. 2013 How linear is wall-bounded turbulence? *Phys. Fluids.* **25**, 110814, p. 20.
JIMENEZ, J. 2018 Coherent structures is wall-bounded turbulence. *J. Fluid Mech.* **842**, P1.
JIMENEZ, J. & PINELLI, A. 1999 The autonomous cycle of near-wall turbulence. *J. Fluid Mech.* **389**, 335–359.
KELVIN, L. 1887 Stability of fluid motion: rectilinear motion of viscous fluid between two parallel plates. *Phil. Mag.* **24** (5), 188–196.
KERSWELL, R.R. 1993 The instability of precessing flow. *Geophys. Astrophys. Fluid Dyn.* **72**, 107–144.
KLINE, S.J., REYNOLDS, W.C., SCHRAUB, F.A. & RUNDSTADLER, P.W. 1967 The structure of turbulent boundary layers. *J. Fluid Mech.* **30**, 741–773.
LAGNADO, R.R., PHAN-THIEN, N. & LEAL, L.G. 1985 The stability of two-dimensional linear flows of an Oldroyd-type fluid. *J. Non-Newtonian Fluid Mech.* **18**, 25–59.
LANDAHL, M. 1980 A note on an algebraic instability of inviscid parallel shear flows. *J. Fluid Mech.* **98**, 243–251.
LANDMAN, M.J. & SAFFMAN, P.G. 1987 The 3-dimensional instability of strained vortices in a viscous-fluid. *Phys. Fluids.* **30**, 2339–2342.
LEBLANC, S. & CAMBON, C. 1997 On the three-dimensional instabilities of plane flows subjected to Coriolis force. *Phys. Fluids.* **9**, 1307–1316.
LOZANO-DURÁN, A., CONSTANTINOU, N.C., NIKOLAIDIS, M.-A. & KARP, M. 2021 Cause-and-effect of linear mechanisms sustaining wall turbulence. *J. Fluid Mech.* **914**, A8.
MARCHIORO, C. 1986 An example of absence of turbulence for any reynolds number. *Commun. Math. Phys.* **105**, 99–106.
MARCUS, P.S. & PRESS, W.H. 1977 On Green's functions for small disturbances of plane Couette flow. *J. Fluid Mech.* **79**, 525–534.
MARKEVICIUTE, V.K. & KERSWELL, R.R. 2024 Threshold transient growth as a criterion for turbulent mean profiles. *J. Fluid Mech.* **996**, A32.
MESHALKIN, L.D. & SINAI, YA G. 1961 Investigation of stability of steady-state solution of a system of equations for the plane motion of an incompressible viscous fluid. *Prikl. Mat. Mekh.* **25**, 1140–1143.
MIYAZAKI, T. & FUKUMOTO, Y. 1992 3-dimensional instability of strained vortices in a stable stratified fluid. *Phys. Fluids.* **4**, 2515–2522.
Moffatt, H. 1967 *The interaction of turbulence with strong shear*. Moscow, June 1965, (ed. A.M. Yaglom and V.I. Tatarsky) Nauka, Moscow, 1967.
ORR, W.M. 1907 The stability or instability of the steady motions of a perfect liquid and of a viscous liquid. part ii: a viscous liquid. *Proc. R. Ir. Acad. Sect. A* **27**, 69.
PANTON, R.L. 2001 Overview of the self-sustaining mechanisms of wall turbulence. *Prog. Aerop. Sci.* **37**, 341–383.
RICHARDSON, L.F. 1922 *Weather Prediction by Numerical Process*. Cambridge University Press.
ROBINSON, S.K. 1991 Coherent motions in the turbulent boundary layer. *Annu. Rev, Fluid Mech.* **23**, 601–639.
SALHI, A. & CAMBON, C. 2010 Stability of rotating stratified shear flow: an analytical study. *Phys. Rev. E.* **81**, 026302.
SCHOPPA, W. & HUSSAIN, F. 2002 Coherent structure generation in near-wall turbulence. *J. Fluid Mech.* **453** (1), 57–108.
SIVASHINSKY, G.I. 1985 Weak turbulence in periodic flows. *Physica D* **17**, 243–255.
SMITS, A.J., MCKEON, B.J. & MARUSIC, I. 2011 High-reynolds number wall turbulence. *Annu. Rev. Fluid Mech.* **43**, 353–375.
SWEARINGEN, J.D. & BLACKWELDER, R.F. 1987 The growth and breakdown of streamwise vorices in the presence of a wall. *J. Fluid Mech.* **182**, 255–290.
TUNG, K.K. 1983 Initial-value problems for Rossbywaves in a shear-flow with critical-level. *J. Fluid Mech.* **133**, 443–469.
WALEFFE, F. 1990 The 3-dimensional instability of strained vortices. *Phys. Fluids.* **2**, 76–80.
WALEFFE, F. 1997 On the self-sustaining process in shear flows. *Phys. Fluids.* **9**, 883–900.

https://doi.org/10.1017/jfm.2025.10571 Published online by Cambridge University Press